Design and Implementation of a Biomolecular Concentration Tracker

Victoria Hsiao,*,† Emmanuel L. C. de los Santos,† Weston R. Whitaker,‡ John E. Dueber,¶ and Richard M. Murray†,§

†Division of Biology and Biological Engineering, California Institute of Technology, Pasadena, California United States
‡Department of Microbiology and Immunology, Stanford University, Palo Alto, California United States
¶Department of Bioengineering, University of California, Berkeley, California United States
§Department of Control and Dynamical Systems, California Institute of Technology, Pasadena, California United States

Ⓢ Supporting Information

ABSTRACT: As a field, synthetic biology strives to engineer increasingly complex artificial systems in living cells. Active feedback in closed loop systems offers a dynamic and adaptive way to ensure constant relative activity independent of intrinsic and extrinsic noise. In this work, we use synthetic protein scaffolds as a modular and tunable mechanism for concentration tracking through negative feedback. Input to the circuit initiates scaffold production, leading to colocalization of a two-component system and resulting in the production of an inhibitory antiscaffold protein. Using a combination of modeling and experimental work, we show that the biomolecular concentration tracker circuit achieves dynamic protein concentration tracking in *Escherichia coli* and that steady state outputs can be tuned.

KEYWORDS: *feedback circuits, negative feedback, synthetic protein scaffolds, two-component systems, live-cell tracking*

RESULTS AND DISCUSSION
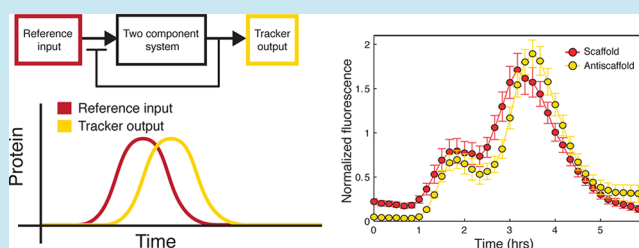
Implementation of reliable feedback and control in engineered circuits is a continuing challenge in synthetic biology. Though positive and negative feedback systems are an essential feature of natural biological networks, synthetic circuits more commonly rely on library-based screening to find optimal expression levels. Not only are the resulting systems sensitive to relative concentrations between components, but each time the circuit is expanded, the network of regulatory sequences must be reoptimized to account for increased load on cell machinery.[1] More importantly, this type of open loop approach only optimizes for a single set of environmental parameters, and inherently does not accommodate stochastic cell-to-cell variation, changes due to cell growth cycles, or changes in cell loading from other circuit modules.[2]

Closed loop systems provide regulation of individual components that is robust with respect to environmental disturbances. Negative feedback is a common feature of natural pathways and has been shown to decrease transcriptional response time,[3] to provide stability and reduce fluctuations,[4] and to be necessary for oscillatory behavior.[5]

Active feedback in biological systems has been previously considered at various levels. Recent studies have designed and studied an RNA-based rate regulating circuit with two opposing negative feedback loops,[6] a system utilizing an RNA binding protein to repress translation of its own mRNA,[7] and analysis of noise in transcriptional negative feedback.[8] There have also been demonstrations of an *in silico* closed loop system, in which a computer measured fluorescence output and automatically modulated the activity of a photosensitive transcription factor.[9] In that study, the negative feedback occurred in the software control system outside of the cell.

In this work, we present an *in vivo* protein concentration tracker circuit. To our best knowledge, this is the first demonstration of dynamic molecular tracking entirely within the cell environment. This circuit contains a single negative feedback loop implemented with scaffold proteins and operates on the time scale of one cell cycle. We show that negative feedback implemented through sequestration results in "tracking" behavior: the proportional modulation of one protein concentration (the *antiscaffold*) relative to that of the reference protein (the *scaffold*) over a range of reference induction levels.

RESULTS AND DISCUSSION

Scaffold-Based Circuit Design and Implementation. Previously, Whitaker et al.[10] designed a scaffold-dependent two-component system in which the phosphotransfer was mediated by a synthetic scaffold protein consisting of small protein—protein binding domains. They demonstrated that weak natural cross-talk between a noncognate histidine kinase and response regulator pair could be artificially amplified via colocalization onto the scaffold. By fusing the kinase to the Crk SH3 domain and the response regulator to half of a leucine zipper, both
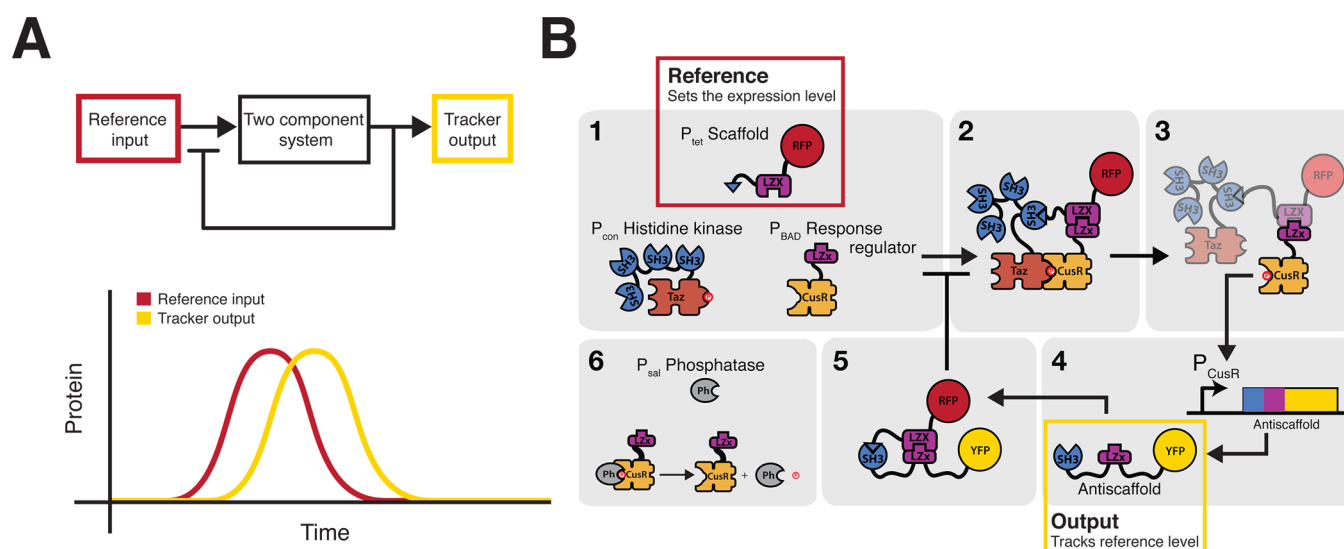
Figure 1. Overview of circuit design. (A) The circuit takes an input that sets the reference value. The input proportionally modulates activity of a two-component signaling system that then produces an output. The output triggers a negative feedback response. The negative feedback is the mechanism that generates real-time tracking behavior. (B) The specific implementation of the circuit is shown. The circuit regulates the production of the amount of target protein (antiscaffold−YFP) with respect to the amount of reference protein (scaffold−RFP). Expression of the target is dependent on the amount of free scaffold. The target contains domains that sequester free scaffold creating a negative feedback loop. Scaffold, response regulator, and phosphatase concentrations are induced via P_{tet}, P_{BAD}, and P_{sal}, respectively.

would be recruited in the presence of a scaffold protein consisting of the SH3 ligand and the other half of the leucine zipper. Forcing the kinase and response regulator into close proximity greatly enhances the level of phosphotransfer and thus the level of downstream expression. The kinase−regulator pair of Taz and CusR was chosen because of measured low levels of cross-talk upon long incubations of purified proteins.[11]

Building upon this scaffold-dependent two-component system, we designed a negative feedback circuit by introducing an antiscaffold molecule that competitively inhibits scaffold function. The *scaffold* molecule consists of a leucine zipper domain (LZX) linked to the SH3 ligand via flexible glycine−serine repeats (Figure 1). The two-component system is composed of the chimeric kinase Taz linked to four SH3 domains and the response regulator CusR linked to a single leucine zipper (LZx) domain (Figure 1A). The presence of the scaffold recruits the HK Taz and RR CusR into close proximity by forming a ternary complex, resulting in the phosphorylation of CusR. The phosphorylated CusR becomes an active transcription factor, binding to its natural promoter (P_{CusR}) and activating expression of the *antiscaffold* protein (Figure 1B). The antiscaffold consists of the complementary LZx and SH3 ligand domains, which allow it to competitively bind to and consequently sequester the scaffold protein ($K_d = 6$ nM for the leucine zipper and $K_d = 100$ nM for the SH3 domain[12,13]). This prevents further phosphorylation of the response regulator, and halts further production of the antiscaffold. In the absence of any scaffold protein, no activated response regulator activity is observed (Supplementary Figure S2, Supporting Information).

We implemented the circuit in a ΔCusS ΔCusR *Escherichia coli* knockout strain.[10] In the absence of CusS, the native bifunctional histidine kinase/phosphatase partner for CusR, activated CusR proteins remain phosphorylated. Accordingly, we reintroduced a CusS(G448A) mutant behind an inducible promoter to tune response regulator deactivation. The G448A mutation disrupts the ATP binding site, eliminating kinase

autophosphorylation without affecting phosphatase activity.[14,15] This created a tunable phosphate sink in our circuit and ensures tight coupling between present scaffold and activated response regulator concentrations. The negative feedback circuit with the antiscaffold is referred to as the *closed loop circuit*. As a control, we also built an *open loop circuit*, in which instead of P_{CusR}-driven expression of the antiscaffold only the antiscaffold reporter is expressed.

We constructed the circuit as a three plasmid system, in which the kinase is constitutively expressed and the scaffold, response regulator, and phosphatase were cloned behind the inducible promoters P_{tet}, P_{BAD}, and P_{sal}, respectively. Dynamic tracking behavior was visualized by adding medium strength ssrA degradation tags (C-terminal, RPAANDENYAAAV) to the scaffold−red fluorescent protein (RFP) and antiscaffold−yellow fluorescent protein (YFP) fusion proteins.[16] The fluorescent reporters mCherry RFP and Venus YFP were chosen on account of their similar maturation times (~5 and 15 min, respectively).[17,18]

Modeling Dynamics and Steady State Circuit Behavior. The circuit was modeled using differential equations with all chemical reactions between species explicitly defined. The model omits transcriptional activity and accounts only for protein level behavior. With the exception of the antiscaffold production term, all other terms are derived from mass action kinetics. A basic model of the circuit was previously published.[19] Here, we have expanded the model by adding the phosphatase species and all accompanying reactions. The 25 species arise from combinations of scaffold (Sc), response regulator (RR), histidine kinase (HK), antiscaffold (AS), and phosphatase (Ph) binding complexes. In total, the model consists of 80 reactions, 25 differential equations, and 26 parameters (See Supporting Information for a complete list of chemical reactions). Many parameters (Table 1) were selected from experimental values found in the literature,[20−22] and others were estimated within a physiologically reasonable range.

Table 1. Table of Model Parameters[a]

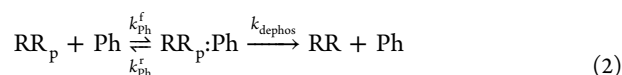| parameter		value	units	description
HK_{tot}		100	nM	histidine kinase
RR_{tot}		0−3000	nM	response regulator
Sc_{tot}		0−5000	nM	scaffold
Ph_{tot}		0−5000	nM	phosphatase
β_{AS}		10	nM s^{-1}	transcription + translation
β_0		0.01		leaky promoter activity (1% of total induction)
γ		3.84×10^{-4}	s^{-1}	deg/dilution[21,27]
γ_{ssrA}		1.5γ	s^{-1}	degradation for ssrA-tagged proteins
n		2		Hill coefficient for antiscaffold activation
K_D		1	nM	K_D for AS activation
k_{dephos}		0.003	s^{-1}	phosphatase mediated dephosphorylation[21]
r		2.8×10^{-4}	s^{-1}	Decay constant for diffusion of inducer[27]
Forward and Reverse Reaction Rates				
k_{HK_p}	k_f	0.003	s^{-1}	HK autophosphorylation[21]
	k_r	0.0001	s^{-1}	ref 20
k_{cogp}	k_f	102.1	s^{-1}	cognate HK-RR phosphorylation[21]
	k_r	0.00294	s^{-1}	ref 21
k_{noncog}	k_f	0.0031	s^{-1} M^{-1}	noncognate HK-RR phosphorylation[21]
	k_r	0.0002	s^{-1} M^{-1}	ref 21
k_{SH3}	k_f	1×10^5	s^{-1} M^{-1}	SH3 domain/ligand binding[22]
	k_r	$k_{f:SH3}$ (0.1×10^{-6})	s^{-1}	$K_D = 0.1\ \mu$M[13]
k_{LZX}	k_f	1×10^5	s^{-1} M^{-1}	leucine zipper binding
	k_r	$k_{f:LZX}$ (0.01×10^{-6})	s^{-1}	$K_D = 0.01\ \mu$M[13]
$k_{Sc:HK}$	k_f	$4k_{f:SH3}$	s^{-1} M^{-1}	scaffold binding to HK with 4 SH3 domains
	k_r	$k_{r:SH3}$	s^{-1}	
$k_{Sc:RR}$	k_f	$k_{f:LZX}$	s^{-1} M^{-1}	scaffold binding to RR with 1 LZX domain
	k_r	$k_{r:LZX}$	s^{-1}	
$k_{ph:RR}$	k_f	1×10^5	s^{-1} M^{-1}	phosphatase binding to RR$_p$
	k_r	1×10^3	s^{-1}	
Closed Loop Antiscaffold Interactions				
$k_{Sc:AS}$	k_f	$k_{f:LZX} + k_{f:SH3}$	s^{-1} M^{-1}	scaffold binding to antiscaffold
	k_r	$0.001k_{r:LZX}$	s^{-1}	
$k_{AS\text{-}SH3}$	k_f	$k_{f:SH3}$	s^{-1}	antiscaffold binding to Sc:RR complex
	k_r	$0.001k_{r:SH3}$	s^{-1}	
$k_{AS\text{-}LZX}$	k_f	$k_{f:LZX}$	s^{-1} M^{-1}	antiscaffold binding to Sc:HK complex
	k_r	$0.001k_{r:LZX}$	s^{-1}	

[a]Parameters estimated from the literature are cited. Note: In the open loop circuit there is no antiscaffold, so the closed loop antiscaffold interaction rates are all zero.

Model reactions can be classified into five categories: production and degradation, phosphorylation, scaffold complex formation, activation, and irreversible sequestration. Phosphorylated species are denoted with a subscript p (e.g., RR$_p$), and complexes are denoted with a colon separating the participating species (e.g., Sc:AS). Though the possibility of modeling the scaffold as an enzyme-like species was considered, we could not assume that either the kinase or the response regulator would always be in excess, a requirement of the substrate in a Michaelis−Menten reaction. Therefore, Michaelis−Menten kinetics were deliberately avoided.
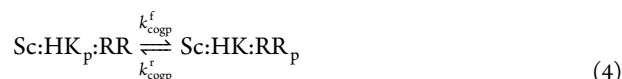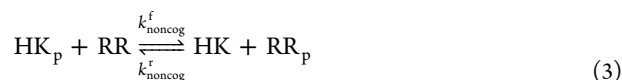
The production rate, β, of the scaffold, histidine kinase, response regulator, and phosphatase are determined by user input of the total steady state value (in nanomolar) multiplied

by the degradation/dilution rate, γ. This ensures constant concentration of these species in solution. The degradation rate γ is applied universally for all species and is estimated based on a cell division time of 30 min.[21]
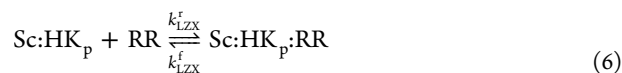
The phosphorylation reactions describe the autophosphorylation of HK and dephosphorylation of RR$_p$. Key reactions that describe this process are

$$\text{HK} \underset{k^r_{HK_p}}{\overset{k^f_{HK_p}}{\rightleftharpoons}} \text{HK}_p \tag{1}$$

$$\text{RR}_p + \text{Ph} \underset{k^r_{Ph}}{\overset{k^f_{Ph}}{\rightleftharpoons}} \text{RR}_p\text{:Ph} \xrightarrow{k_{dephos}} \text{RR} + \text{Ph} \tag{2}$$

The phosphatase forms a complex with the RR$_p$ prior to dephosphorylation. We model both phosphorylation and dephosphorylation with a two-step reaction model, an approach consistent with previous models.[23] Rate constants for kinase phosphorylation and dephosphorylation of the response regulator were chosen based on cognate and noncognate phosphorylation rates measured for natural two-component systems and occur on the order of seconds.[21] The following equations show phosphorylation in the absence and presence of scaffold:

$$\text{HK}_p + \text{RR} \underset{k^r_{noncog}}{\overset{k^f_{noncog}}{\rightleftharpoons}} \text{HK} + \text{RR}_p \tag{3}$$

$$\text{Sc:HK}_p\text{:RR} \underset{k^r_{cogp}}{\overset{k^f_{cogp}}{\rightleftharpoons}} \text{Sc:HK:RR}_p \tag{4}$$

Reaction rates for scaffold complex formation were based on the kinetics of the protein−protein interaction domains SH3 domain/ligand and LZX/LZx. SH3 domain/ligand binding has an estimated association affinity K_d of 0.1 μM, while leucine zippers have a K_d of approximately 0.01 μM.[12,13,24,25] Here we have examples of histidine kinase and response regulator binding to scaffold via SH3 and LZX binding, respectively:

$$\text{Sc} + \text{HK}_p \underset{k^r_{SH3}}{\overset{4k^f_{SH3}}{\rightleftharpoons}} \text{Sc:HK}_p \tag{5}$$

$$\text{Sc:HK}_p + \text{RR} \underset{k^f_{LZX}}{\overset{k^r_{LZX}}{\rightleftharpoons}} \text{Sc:HK}_p\text{:RR} \tag{6}$$

A phosphorylated response regulator becomes an active transcription factor. We considered all possible complexes with RR$_p$ as possible activators (shown as RR$_{active}$). Since the response regulator, CusR, dimerizes upon phosphorylation, the total rate of AS production, k_{fAS}, is modeled as a second-order Hill function:

$$\phi \xrightarrow{k_{fAS}} \text{AS} \tag{7}$$

$$k_{fAS} = \beta_{AS}\left[\beta_0 + \left(\frac{\text{RR}_{active}^2}{K_D^2 + \text{RR}_{active}^2}\right)\right] \tag{8}$$

where RR$_{active}$ = RR$_p$ + Sc:RR$_p$ + Sc:HK:RR$_p$ + Sc:HK$_p$:RR$_p$ + Sc:RR$_p$:AS.

The negative feedback component comes about through the irreversible sequestration of the scaffold once it has bound to the antiscaffold. We made the assumption that the individual SH3 and LZX domains on the antiscaffold bind independently,
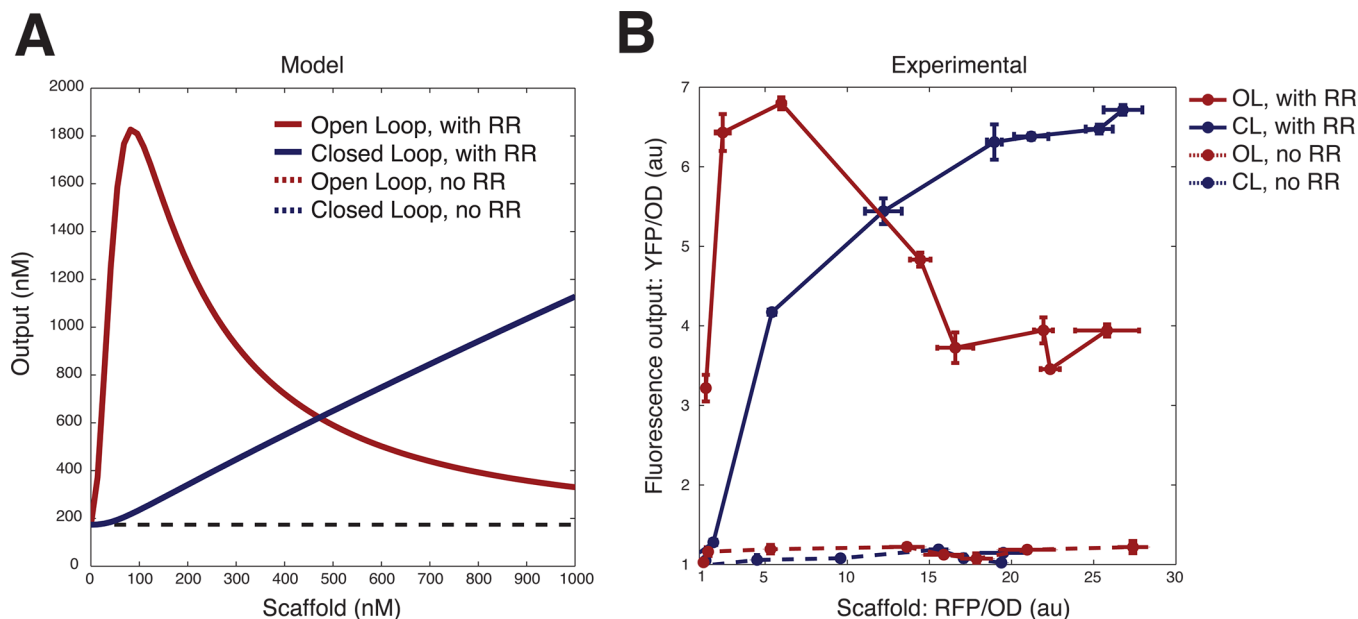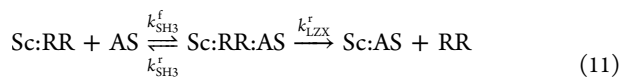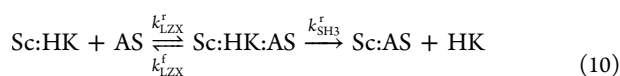
Figure 2. Open loop versus closed loop. (A) Model predictions of scaffold circuit with and without negative feedback. Solid lines show antiscaffold output over a range of scaffold concentrations (0−1000 nM) for open and closed loop circuits with constant response regulator (100 nM). Dotted lines show lack of output in the absence of response regulator. Open loop circuit shows scaffold single occupancy effect at lower levels of scaffold. (B) Steady state experimental data of open and closed loop circuits with and without response regulator matches model predictions. Both sets of experimental data were normalized by the autofluorescence of a control *E. coli* strain (Figure S2, Supporting Information).

at the same rates as HK and RR binding. However, once either the SH3 or LZX component of the AS has bound to the Sc, this results in a local concentration of the free domain that is substantially higher than the K_D. Therefore, we assume that the other domain quickly displaces any competing species and sequesters the entire Sc. The effective irreversibility comes about through steric hindrance of competing HK and RR species, both of which only have one compatible binding domain to the Sc:

$$Sc + AS \xrightarrow{k^f_{Sc:AS}} Sc:AS \qquad (9)$$

$$Sc:HK + AS \underset{k^f_{LZX}}{\overset{k^r_{LZX}}{\rightleftharpoons}} Sc:HK:AS \xrightarrow{k^r_{SH3}} Sc:AS + HK \qquad (10)$$

$$Sc:RR + AS \underset{k^r_{SH3}}{\overset{k^f_{SH3}}{\rightleftharpoons}} Sc:RR:AS \xrightarrow{k^r_{LZX}} Sc:AS + RR \qquad (11)$$

The validity of the model was tested by comparing the open and closed loop circuits. In the open loop circuit, the negative feedback binding reactions are set to zero (Table 1). Experimentally, this was done by replacing the antiscaffold with a fluorescent reporter alone. Figure 2A shows simulated steady state values for antiscaffold (or fluorescent reporter) output over a range of scaffold concentrations (0−1000 nM), with either 0 or 100 nM of response regulator. In the cases with no response regulator, the circuit does not function and production of output is solely due to simulated leaky antiscaffold production (β_0). When response regulator molecules are present, the open loop circuit output decreases significantly with increasing scaffold. Though it is not intuitive, this can be explained as the scaffold single occupancy effect,[13,26] where an overabundance of free scaffold leads to binding of only kinase or response regulator but not both. When we examine the prevalence of these intermediate species (Sc:HK, Sc:RR) in simulation, we can see that when the total

concentration of singly bound scaffold increases, decrease in output is indeed observed (Figure S1A, Supporting Information). The same effect also occurs in the closed loop circuit, but much higher concentrations of scaffold are needed, since the antiscaffold sequestration lowers the effective number of free scaffold molecules in solution (Figure S1B, Supporting Information).

Experimental data for the circuit closely recapitulated the model predictions (Figure 2B). First, without induction of RR for both open and closed loop circuits, there is no output YFP. Second, the open loop circuit shows the single scaffold occupancy effect at lower concentrations of scaffold. In the case of no scaffold induction, the open loop circuit has about three times more background than the closed loop circuit. This is due to leakiness in scaffold production in the absence of anhydrotetracycline (aTc). In the closed loop circuit, leaky production of scaffold is subdued by the negative feedback, while in the nonregulated open loop, we see significant production of YFP. All data was normalized to the autofluorescence of a control *E. coli* strain (Figure S2, Supporting Information).

We compared protein expression to fluorescence output to verify the use of fluorescence traces as a proxy for protein concentration. Western blot quantification was done with an analogous circuit containing a bicistronic scaffold (3×FLAG)/RFP and antiscaffold−GFP (3×FLAG) (Figure S3, Supporting Information). mCherry is expressed from its own RBS instead of tethering directly to the scaffold (12 kDa) to provide a substantial size difference from the antiscaffold (44 kDa). Quantification of band intensities show good agreement between antiscaffold expression and measured fluorescence output (Figure S4, Supporting Information). These results served to validate both the model and the use of synthetic scaffolds as a tunable mechanism for negative feedback.

Characterization of Step Response. We characterized circuit response time by testing the closed loop response to
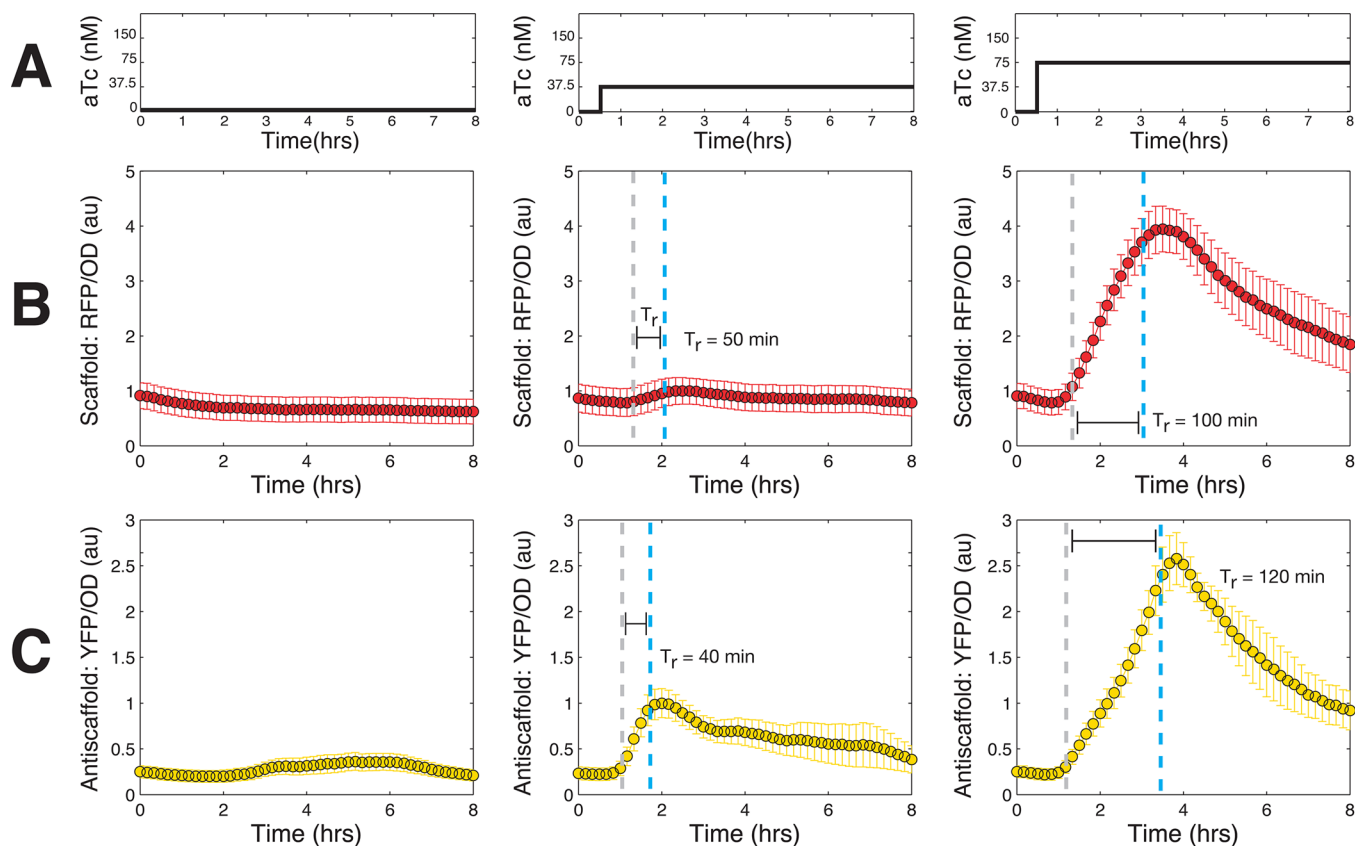
Figure 3. Step induction of closed loop circuit. (A) aTc induction of Sc-RFP began 30 min after start of experiment and continued for the rest of the experiment. (B) scaffold−RFP/OD measurements for no induction (left), 37.5 nM induction (middle), and 75 nM induction (right). Response time (T_r) is quantified by finding the time needed for fluorescence to increase from 10% (gray dotted line) to 90% of the maximum value (blue dotted line). A 2-fold increase in aTc results in a 4-fold increase in scaffold expression and a 2-fold increase in response time. The insets show growth curves for each condition. (C) AS-YFP/OD measurements show 2.5-fold increase between the two inputs and a 3-fold increase in response time. Fluorescent measurements are normalized such that the maximum of the middle column (37.5 nM aTc) is 1 au to better visualize fold change.

step inputs. Using a programmable microfluidic plate (CellAsic) under a microscope, step induction of the scaffold protein was achieved by flowing in 0, 37.5, or 75 nM of aTc (Figure 3A) after 30 min of growth in normal media. Cellular production of response regulator and phosphatase was preinduced by incubating cells with arabinose and salicylate. Microscopy analysis methods are described in Figure S5, Supporting Information. Growth curves for all the conditions are in Figure S7, Supporting Information. In all conditions, expression of scaffold−RFP (Figure 3B) began about 30 min after induction and occurred almost simultaneously with that of antiscaffold−YFP (Figure 3C). Although we had selected mCherry and Venus-YFP on account of their similar maturation times, Venus still matures faster than mCherry (5 and 15 min, respectively). We believe that although there is a delay in mCherry maturation, the scaffold is immediately functional, leading to the near overlap of RFP and YFP expression. In order to better visualize the fold change, fluorescence output is normalized by the maximum value of the lowest step input.

Response times (T_r) for fluorescent detection of scaffold (RFP) and antiscaffold (YFP) were quantified. In control theory, response time is the amount of time needed for an output signal to increase from 10% to 90% of its final steady state. As cells reach stationary phase, circuit expression gradually turns off, and no steady state in fluorescence output is maintained. The 0 nM aTc case shows basal expression of the

fluorescent proteins. We observed that scaffold induction, regulated by a P_{tet} promoter, has a 4-fold expression increase between 37.5 nM (Figure 3C) and 75 nM (Figure 3D) induction, but only a 2-fold increase in response time (from 50 to 100 min). Antiscaffold output, regulated by the scaffold concentration, shows a 2.5-fold increase in maximum expression and a 3-fold increase in response time (from 40 to 120 min).

This step input characterization revealed that scaffold and antiscaffold fluorescence could be observed almost simultaneously about one cell cycle (30 min) after aTc induction of scaffold transcription. Following induction of the circuit, the response time to maximum expression increases in a linear-like fashion with increasing scaffold induction.

Circuit Closely Follows Three Step Induction. Following step input characterization, we investigated circuit response to multiple step-up inputs. Figure 4 shows the results of a three step scaffold induction experiment with 1 h steps corresponding to 50 nM increases of aTc inducer. Growth curves are shown in Figure S8, Supporting Information. The single negative feedback loop in the circuit represses overproduction of antiscaffold, but there is no mechanism for feedback in the case of an excess of scaffold or antiscaffold. As such, the model predicts that increases in inducer will lead to immediate increases of scaffold followed closely by the antiscaffold but once induction is turned off, degradation of proteins depends on the endogenous ClpXP degradation machinery (Figure 4A).
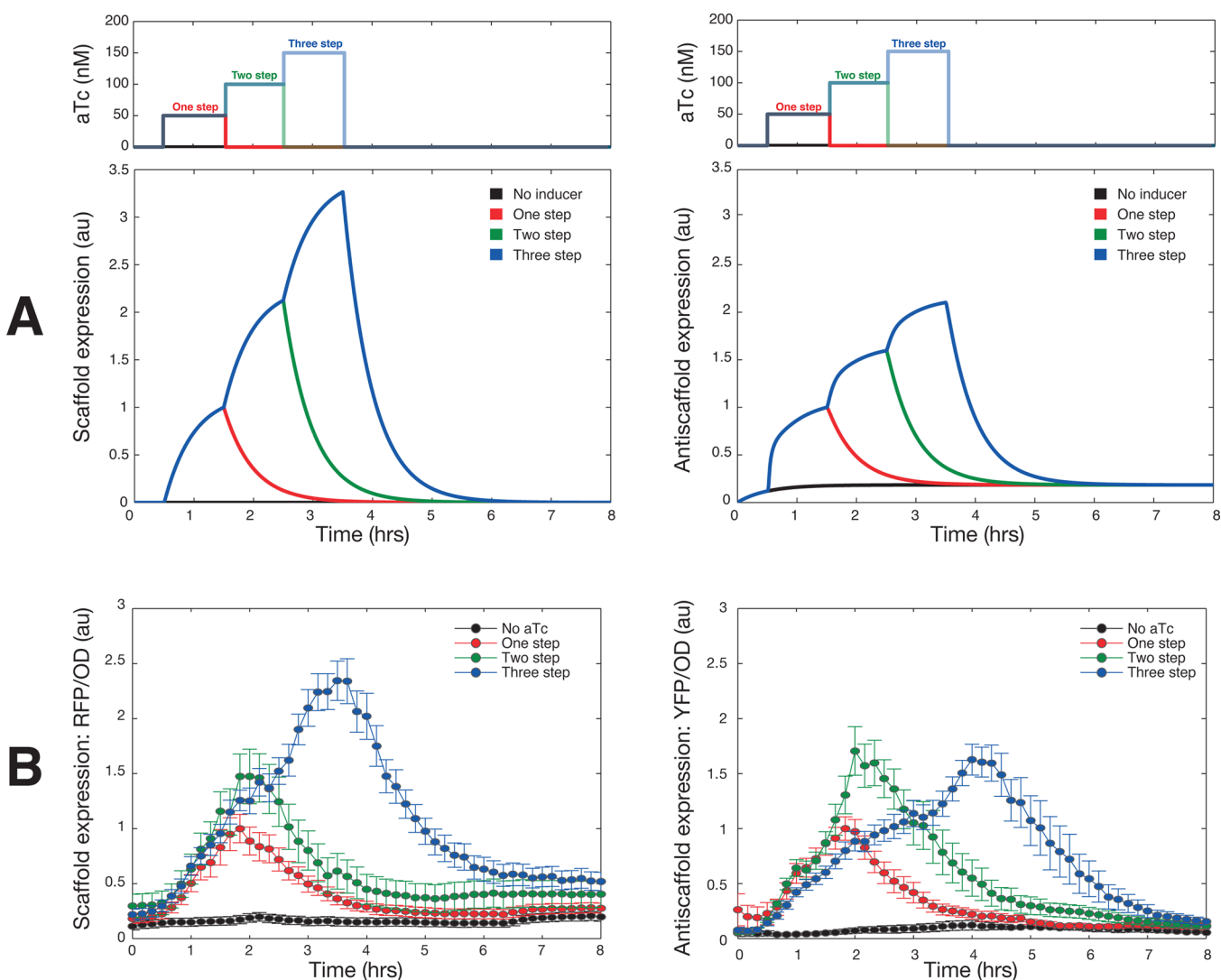
Figure 4. Multistep induction of tracker circuit. (A) Simulation results for a three step induction show overlapping response times with each curve decreasing based on degradation rate after induction ceases. Upper panel shows aTc induction pattern with 1 h steps increasing in 50 nM increments starting 30 min after start of experiment. (B) Experimental time traces for Sc-RFP show overlapping fluorescence output, with each curve decreasing at a time proportional to the number of steps. Corresponding antiscaffold−YFP data show similar overlaps and proportional decreases. Fluorescent measurements are normalized such that the maximum value of the one step curve is 1 au to better visualize fold change. Growth curves are shown in Figure S8, Supporting Information.

Additionally, the upward slope of each curve should overlap until induction ceases.

Step-up induction was performed on cells preincubated in arabinose and salicylate, activating expression of response regulator and phosphatase, respectively. As shown in Figure 4B, experimental results for a three step induction are consistent with model predictions and show overlapping curves during the ascent, with each individual curve dropping off slowly as induction ceases. The chemical induction of the scaffold produces a much smoother output curve compared with the response regulator-modulated antiscaffold. Due to high levels of leaky expression, the open loop circuit did not respond to multistep inductions (Figure S8, Supporting Information).

Inducer Diffusion Rates Contribute to Cumulative Effect of Sequential Pulses. We observed in our model that variations in inducer diffusion rate would greatly affect the outcome of sequential pulses (Figure 5A). The removal of aTc from the cytoplasm and surrounding media is not instantaneous, and induction does not go to zero. Growth curves are

shown in Figure S9, Supporting Information. Given two sequential 30 min pulses spaced 1 h apart, the diffusion constant determined whether two independent, identical outputs occurred or an additive effect would take place. Essentially, if the first pulse of inducer is not given sufficient time to diffusion out of environment, aTc molecules from the first pulse are still present when the second pulse occurs. We modeled inducer diffusion following a pulse with an exponential decay term, $\beta_{Sc} = \beta_{ind}(-rt)$.[27] Figure 5A shows two pulse simulation results when the default decay constant ($r = 2.8 \times 10^{-4}$ s^{-1}, middle column) is increased or decreased by 10-fold.

When we tested two pulse induction *in vivo* (Figure 5B), we ran simultaneous experiments with zero, one, and two 30 min pulses of aTc (50 nM). The single pulse fluorescence maximum (Figure 5B, middle column) was normalized to 1 au. It is clear from the two pulse fluorescence output data that the diffusion rate of aTc after a pulse *in vivo* was actually much slower than expected *in silico*. In fact, so much of the scaffold from the first pulse remained that there was almost a 2-fold increase in
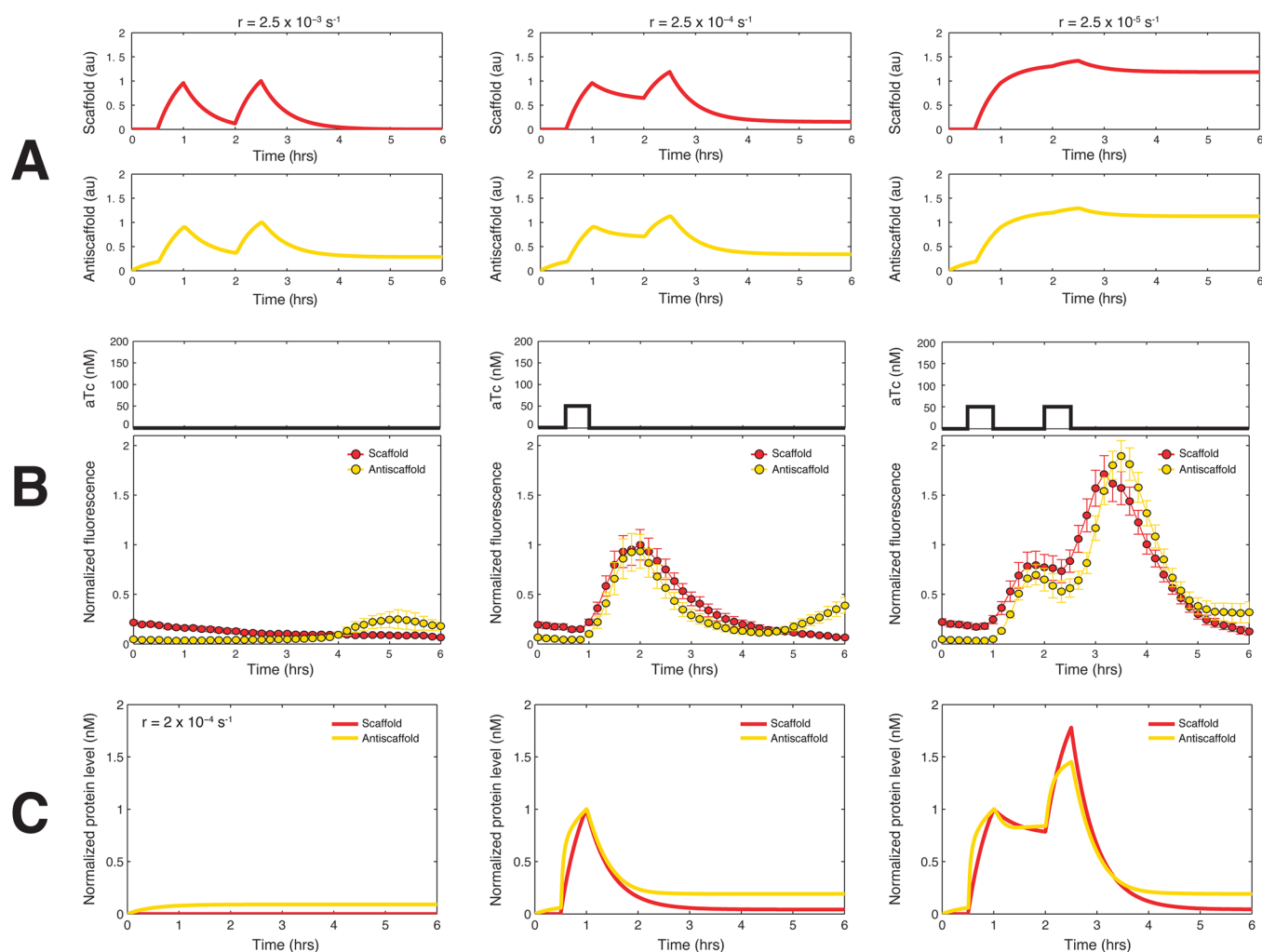
Figure 5. Two pulse induction of circuit. (A) Model results for a range of inducer decay constants from 2.8×10^{-3} to 10^{-5} s^{-1}. Fast diffusion (left) shows two independent pulses, intermediate diffusion (middle) results show some overlapping protein from first and second pulses, and slow diffusion (right) shows large amounts of overlapping protein from the first to the second pulse. (B) Experimental data for zero, one, and two pulses of 50 nM aTc. Data are normalized by maximum of single pulse induction (middle column). (C) Simulations with improved inducer diffusion rates ($r = 2 \times 10^{-4}$ s^{-1}).

maximal expression during the second pulse. This was an effect that had not been apparent previously during the multistep inductions, where we showed sequential increases in inducer concentration. These data show that modulation of pulse frequency, but not concentration, can result in the same additive effect as increasing inducer concentration.

We then sought to improve our model by tuning the inducer decay constant (Figure 5C), generating outputs that demonstrated the nearly 2-fold increase observed *in vivo*. Although the optimized decay rate ($r = 2 \times 10^{-4}$ s^{-1}) better captured gene expression during log phase, we consistently observed a rapid decrease in fluorescence as cells approached stationary phase. We believe this is due to upregulation of ClpX and other ssrA machinery in stationary phase.[28] This resulted in improved model performance when simulating dynamic circuit behavior.

Model-Informed Exploration of Parameter Space. Circuit limitations were explored *in silico*. Specifically, we investigated the effects of tuning response regulator and phosphatase concentrations on the ability of the antiscaffold output to track the scaffold reference. Response regulator and phosphatase concentrations are easily accessible parameters via inducible promoters in our experimental system. In Figure 6A,

a scan of input−output response curves is shown over a range of response regulator and phosphatase concentrations (See Figure S10, Supporting Information, for explicit values). For each curve in the grid, the scaffold concentration in which the single occupancy drop-off occurs was found, and the slope of the curve up to that concentration was found with a linear fit. The maximum scaffold occupancy limit is the concentration of scaffold molecules at which each scaffold molecule only has either a response regulator or histidine kinase. The slope of the curve up to that point represents the antiscaffold to scaffold ratio that can be achieved by the circuit. In the case where the single occupancy limit does not appear, the last concentration is used. Data shown in Figure 6B indicates that increasing response regulator values result in a greater AS/Sc ratio (up to 1.5-fold increase), while increasing phosphatase serves to bring down that ratio. The effect of increasing phosphatase is apparent when the maximum scaffold occupancy limit is examined (Figure 6C). Furthermore, the simulations show that some minimal amount of phosphatase is necessary for a sufficiently high response regulator turnover rate so as to approach a 1:1 ratio. As phosphatase concentration increases, active response regulators are quickly dephosphorylated,
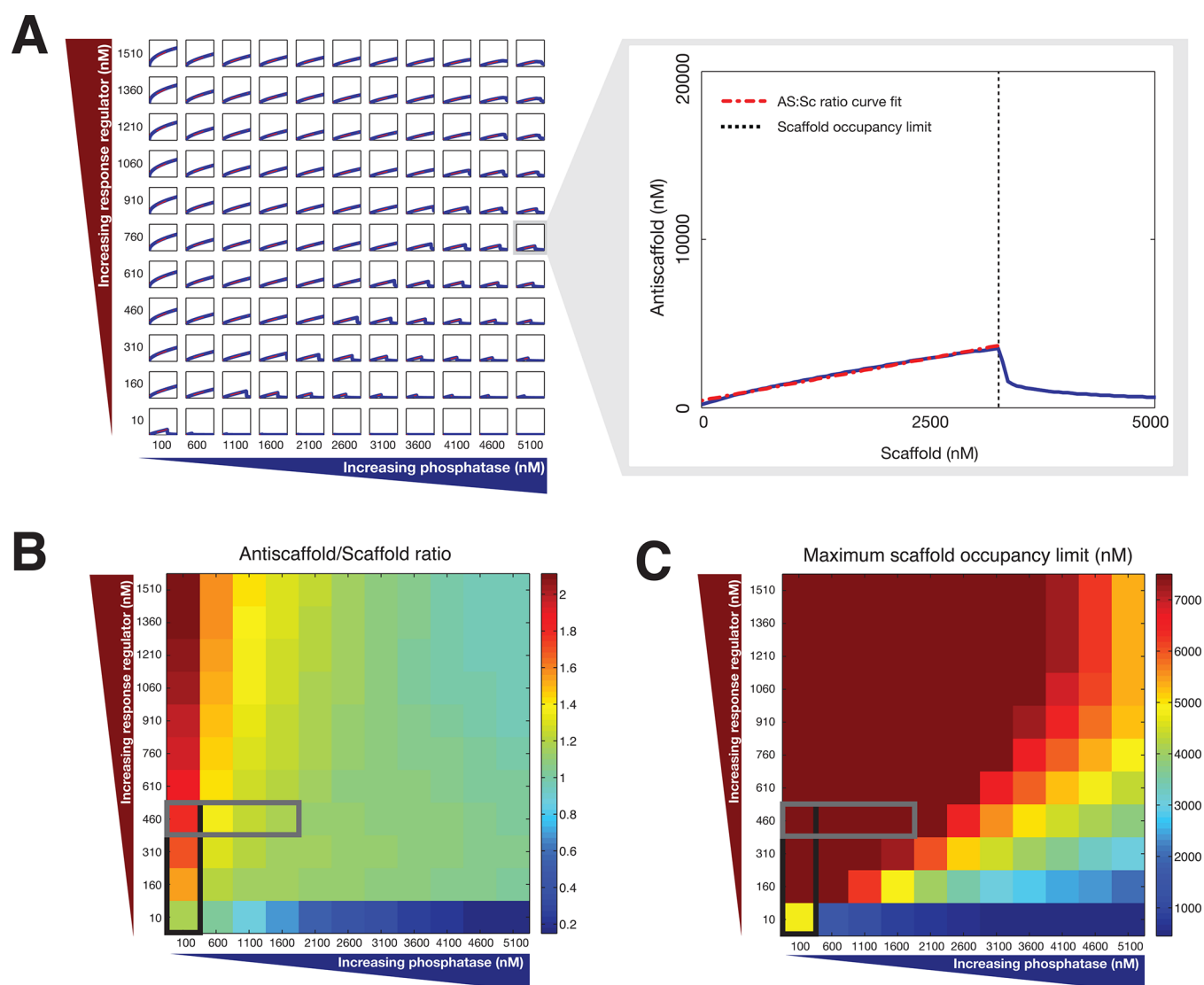
Figure 6. Model-based exploration of parameter space. (A) Simulations of scaffold to antiscaffold inputs and outputs over a range of phosphatase (100−5100 nM, 500 nM increments) and response regulator (10−1510 nM, 150 nM increments) concentrations. Enlargement shows the scaffold single occupancy limit concentration and curve fitting for each curve. Red dotted lines show curve fits; the slope represents the antiscaffold to scaffold ratio. (B) Heat map showing antiscaffold to scaffold ratio for each curve shown in part A. Increasing response regulator results in greater AS/Sc ratios. Gray box represents estimated experimental phosphatase induction range. Black box estimates experimental response regulator induction range. (C) Heat map of maximum scaffold occupancy limit. Higher concentrations of phosphatase result in decreased maximum scaffold occupancy limit.

decreasing the efficacy of the scaffolds, lowering the maximum occupancy concentration, and making the drop-off more steep. Based on experimental outputs of our circuit, however, we believe the actual achievable dynamic range of the circuit is limited to the lower left corner of the parameter space. The qualitatively estimated induction range is shown with the black and gray rectangles in Figure 6B,C.

By modulating response regulator and phosphatase concentrations, a range of maximal expression levels for scaffold and antiscaffold can be achieved. Figure 7A,B shows steady state circuit response to varying levels of response regulator induction in both the model and experimental circuit. Increasing RR concentrations increases the gain of the system by increasing the number of available active transcription factors for the AS promoter. In simulation data (Figure 7A), we see that the scaffold occupancy effect is mitigated by higher levels of response regulator. This is consistent with our

previous explanation, since more regulator means almost all free scaffold molecules will exist as Sc:RR. Experimental data for tuning response regulator concentration via 10-fold increases of arabinose (Figure 7B) do not extend the scaffold levels far enough to show the occupancy effect, but the increasing output gain is evident.

The presence of phosphatase in the circuit modulates the amount of time that phosphorylated response regulator is active. Hence, tuning phosphatase concentrations changes RR ↔ RR_p cycling time. Early versions of the circuit did not include the phosphatase species,[19] and we were unable to observe dynamic behavior due to buildup of RR_p. Using the model, we explored the effects of adding a phosphatase prior to testing *in vivo*. Figure 7C,D shows steady state responses across a range of phosphatase concentrations. Simulation results show that increasing phosphatase decreases overall circuit output (Figure 7C) by decreasing the average time RR_p is active.
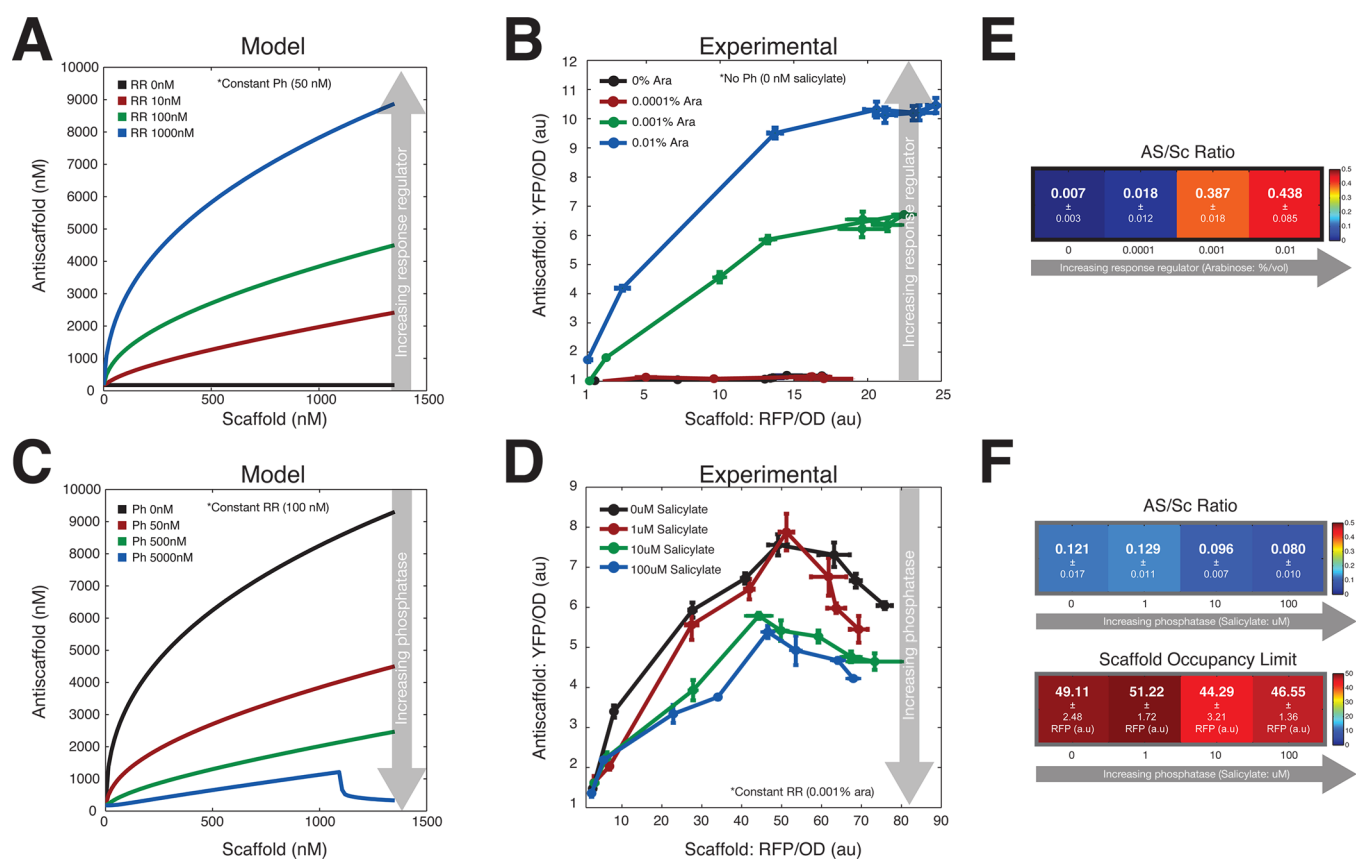
Figure 7. Steady state experimental tuning of response regulator and phosphatase. (A) Simulation data of input−output curves with increasing response regulator concentrations (0−1000 nM). Increasing response regulator increases the scaffold occupancy limit as well as overall AS/Sc ratio. (B) Experimental data of steady state scaffold to antiscaffold curves with 10-fold increases in response regulator induction (0−0.01% arabinose). There was no additional induction of phosphatase (0 nM salicylate). (C) Simulation data of input−output curves with increasing phosphatase concentrations (0−5000 nM) with constant response regulator concentration of 100 nM. Increasing phosphatase decreases the scaffold occupancy limit and overall AS/Sc ratio. (D) Experimental data of steady state circuit behavior with 10-fold increases in salicylate. Response regulator concentration is constant (0−100 μM salicylate). (E) Ratios of YFP/RFP from part B as a proxy for As/Sc ratios with increasing response regulator. Scaffold occupancy limit was not observed in response regulator experiments. (F) Ratios of YFP/RFP and scaffold occupancy limit values from part D with increasing phosphatase. All experimental data was normalized by baseline autofluorescence values.

Experimental results (Figure 7D) support model predictions and show this suppression of output with increased induction via salicylate.

In Figure 7E,F, these experimental steady state data are analyzed using the same techniques shown in Figure 6. Figure 7E shows antiscaffold to scaffold ratio and scaffold occupancy limit as calculated based on RFP/YFP fluorescence data with 10-fold increases in response regulator induction with no phosphatase present. Similar to the analysis used in the model, if the single occupancy drop is not observed, the highest scaffold concentration is taken. Figure 7F shows the same metrics with 10-fold increases in phosphatase induction with constant response regulator (0.001% arabinose induction). Experimental data is presented as a function of fold change from background fluorescence, so it cannot be compared directly with model data (presented in nanomolar). However, the overall trends are in agreement. Because response regulator increases, we see a significant increase in antiscaffold to scaffold ratio and little change in the occupancy limit. With increasing phosphatase, we see a slight decrease in AS/Sc ratio and scaffold occupancy limit. We believe these data show us that our experimental range occupies only a small fraction of that shown by our model (Figure 6B,C) and that these limitations are due to the limited dynamic range of the inducible

promoters (P_{BAD}-RR, P_{sal}-Phos, Figure S11, Supporting Information).

Scaffold-Based Circuits for Rapid Feedback. We have designed a novel negative feedback tracker circuit using modular synthetic scaffold proteins and a two-component system with scaffold-dependent phosphorylation. The use of scaffold proteins for negative feedback could potentially be a robust way of linking modules and ensuring constant performance despite intrinsic and extrinsic noise. Scaffold proteins have been shown to be powerful hubs for organization of regulatory feedback in natural networks, usually by colocalization of phosphorylation machinery.[26] Previous studies have rewired the naturally occurring Ste5 scaffold in the yeast MAPK cascade to redirect signals, to modify delays in signaling time, and to introduce ultrasensitivity.[29,30] The modular scaffold proteins used in this study were previously used to control phosphotransfer to noncognate response regulators, building a synthetic signaling pathway.[13,31,32] Here we have taken those same scaffolding modules and built an entirely synthetic feedback circuit. The system allows for tunable control of output gain and cycling time. Most importantly, the proportional antiscaffold tracking of the scaffold is maintained over a range of component concentrations.

After we designed the circuit framework, we constructed and then experimentally validated an ODE-based mathematical model. Through selection of parameters and reaction rates based on the literature, we obtained a model able to reasonably predict circuit behavior. Comparisons between simulation and experimental data confirmed the presence of scaffold-mediated negative feedback, and we used the model to scan the parameter space in a way that would have been time and resource intensive to explore *in vivo*. We found that steady state circuit gain can be tuned by changing response regulator concentrations and cycling time is controlled by varying phosphatase levels, observations that were supported by experimental data. Following initial step induction system characterization of step input response time, expression of both the reference (Sc-RFP) and output (AS-YFP) protein was shown to be fast and responsive to multistep inputs. Finally, we found that pulse-modulated induction could result in additive circuit response, leading to improvement of the model through more accurate inducer diffusion parameter values.

A scaffold-based biomolecular tracking circuit has potential applications in active regulation of component expression in synthetic circuits. The relatively small size (approximately 60 AA) of the scaffold and antiscaffold proteins facilitates attachment to larger proteins, represented in this work by mCherry-RFP and Venus-YFP. Rather than open loop tuning of regulatory sequences and large-scale screening, scaffold-based negative feedback could be utilized. By attaching the scaffold to a native protein, it may also be possible to tie synthetic circuit inputs to naturally occurring cycles *in vivo*. It is well-known that many natural cell processes such as developmental segmentation, circadian clocks, and stem cell multipotency involve oscillatory gene expression.[33,34]

Furthermore, response to signal transduction may be modulated not by amplitude, but by frequency.[35] We have shown that the scaffold-modulated protein tracker follows changes in both amplitude and frequency and exhibits good agreement with a mass-action model. Future iterations of this design may improve tracking fidelity by including reverse feedback loop to compensate for overexpression.

■ METHODS

Cell Strain and Media. The circuit was implemented in the *E. coli* cell strain WW62, a variant of BW27783 (CGSC 12119) with knockouts of EnvZ, OmpR, CusS, CusR, CpxA, and CpxR. All cell culture was done in optically clear MOPS EZ Rich defined medium (Teknova, M2105), with 0.4% glycerol instead of 0.2% glucose. The use of glycerol as a carbon source was done to prevent interference with the arabinose induction of the P_{BAD} promoter.

Tested arabinose induction levels were 0, 0.0001%, 0.001%, 0.01%, and 0.1% (20% stock solution). Anhydrotetracycline (aTc) was diluted in media at concentrations of 0, 5, 15, 30, 60, 90, 120, and 150 nM. Sodium salicylate was resuspended at a stock concentration of 100 mM and diluted 1:1000 in media for experiments.

Plasmids. Plasmids used in this study were derived from those used in Whitaker et al.[10] The plasmid encoding the SH3-ligand−LZX−mCherry scaffold (pVH001) has a high copy backbone (ColE1) with ampicillin resistance. The CusR−LZx response regulator and SH3-domain−LZx−VenusYFP antiscaffold plasmids (pVH003 for closed loop, pVH009 for open loop) are on a medium copy backbone (pBBR1) with kanamycin resistance. The 4SH3-domain−Taz histidine kinase

and CusS-G448A phosphatase are on a low copy plasmid (p15A) with chloramphenicol resistance. Detailed plasmid maps are shown in Figure S11, Supporting Information, and a complete list of plasmids and strains can also be found in the Supporting Information.

Plate Reader Experiments. Plate reader data were collected on a Biotek H1MF machine using the kinetic read feature. Cell were grown in two consecutive overnight cultures in MOPS EZ rich media. On the day of the experiment, overnight cultures were diluted 1:40 and grown to OD ≈ 0.1 prior to the start of the experiment. Cells were incubated in the plate reader at 37 °C and shaken at 800 rpm between reads. Measurements were taken every 5 min. Cells were grown in clear bottomed 96-well microplates (PerkinElmer, ViewPlate, 6005182) and sealed with breathable clear membranes (Sigma-Aldrich, Breath-Easy, Z380059). mCherry was read at excitation/emission of 580/610 nm at a gain setting of 140, Venus was read at 500/540 nm at a gain setting of 100, GFP was read at 488/525 nm at a gain setting of 75.

Analysis of the data was done by taking fluorescence readings at late log phase for each independent well. Experimental conditions were done in triplicate and repeats were averaged. Fluorescence per OD was normalized by the fluorescence of a control strain (lacking mCherry/YFP/GFP) such that the cell autofluorescence equals 1 au (Figure S2, Supporting Information). Error bars shown are standard error of the mean.

Western Blots. Cultures were grown for 5 h in a deep-well microplate at 37 °C with a range of aTc from 0−120 nM. Arabinose was kept constant at 0.001%. No salicylate was used. After 5 h, OD600, RFP, and GFP were measured in a plate-reader. Western blot samples were collected and spun down. Because aTc concentration can affect growth rates, the volume spun down was calculated based on OD to ensure consistent cell mass. Pellets were resuspended in lysis buffer and boiled for 10 min. Samples were run on 4−20% tris-glycine gels (Novex, 150 V for 1 h), and a semidry transfer apparatus was used (Bio-Rad, 15 V for 20 min) to transfer onto a PVDF membrane. Monoclonal anti-FLAG M2-peroxidase (HRP) antibody was diluted 1:88,000 in 5% milk. Blot imaging was done using the Chemi Hi Resolution setting on a BioRad ChemiDoc MP imager. Quantification of band intensity was done using Image Lab 5.0 (BioRad).

Microscopy. Step induction data were taken using the CellAsic ONIX microfluidic perfusion system for bacteria (B04A). The microscope is an Olympus IX81-ZDC enclosed in a custom heater box. Images were taken using a 100× oil immersion phase objective. Fluorescence filters are 580/630 nm for mCherry (Chroma 41027) and 510/560 nm for YFP (Chroma 31040 JP2). Microscope media was augmented with oxidative scavengers Trolox (200 nM) and sodium ascorbate (2 mM).

Overnight cultures were then diluted 1:500 in media containing arabinose (0.01%) or salicylate (100 μM) or both 4 h prior to loading in the CellAsic plate. This is to ensure steady state concentrations of response regulator and phosphatase prior to aTc induction of the scaffold. Cells were diluted 1:10 again before loading. Microscopy movies were taken inside a temperature controlled environment set at 37 °C, and images were taken at 10 min intervals. Exposure time was 10 ms for brightfield and 500 ms for mCherry and YFP fluorescent channels.

Analysis of microscope movies was done using custom algorithms in ImageJ and MATLAB. For each frame, the phase

image is converted to a binary mask of the cell colony. The mask is then used to find total mCherry and YFP fluorescence in the frame. After subtraction of background fluorescence, the total fluorescence is normalized by the total cell area (fluorescence intensity per pixel). For step induction experiments, fluorescence is normalized such that the maximum fluorescence of the lowest concentration induction is equal to 1 au. Figure S5, Supporting Information, shows the microscopy analysis workflow. Error bars shown in microscopy time trace data are the standard error of the mean between analysis of different positions ($n = 7-10$) on the same experimental plate.

Model Implementation. The model was implemented using the Simbiology toolbox in MATLAB and the ode15s solver (See Supporting Information files for MATLAB code).

■ ASSOCIATED CONTENT

Ⓢ Supporting Information

This material is available free of charge via the Internet at http://pubs.acs.org.

■ AUTHOR INFORMATION

Corresponding Author

*E-mail: vhsiao@caltech.edu.

Notes

The authors declare no competing financial interest.

■ ACKNOWLEDGMENTS

■ REFERENCES

(1) Klumpp, S., Zhang, Z., and Hwa, T. (2009) Growth Rate-Dependent Global Effects on Gene Expression in Bacteria. *Cell 139*, 1366−1375.

(2) Cardinale, S., Joachimiak, M. P., and Arkin, A. P. (2013) Effects of Genetic Variation on the *E. coli* Host-Circuit Interface. *Cell Rep. 4*, 231−237.

(3) Rosenfeld, N., Elowitz, M. B., and Alon, U. (2002) Negative Autoregulation Speeds the Response Times of Transcription Networks. *J. Mol. Biol. 323*, 785−793.

(4) Becskei, A., and Serrano, L. (2000) Engineering stability in gene networks by autoregulation. *Nature 405*, 590−593.

(5) Ferrell, J. E., Jr. (2013) Feedback loops and reciprocal regulation: recurring motifs in the systems biology of the cell cycle. *Curr. Opin. Cell Biol.*, 1−11.

(6) Franco, E., Forsberg, P.-O., and Murray, R. M. (2008) Design, modeling and synthesis of an *in vitro* transcription rate regulatory circuit. *Proc. Am. Control Conf.*, 2786−2791.

(7) Stapleton, J. A., Endo, K., Fujita, Y., Hayashi, K., Takinoue, M., Saito, H., and Inoue, T. (2012) Feedback Control of Protein Expression in Mammalian Cells by Tunable Synthetic Translational Inhibition. *ACS Synth. Biol. 1*, 83−88.

(8) Dublanche, Y., Michalodimitrakis, K., Kümmerer, N., Foglierini, M., and Serrano, L. (2006) Noise in transcription negative feedback loops: simulation and experimental analysis. *Mol. Syst. Biol. 2*, No. 41.

(9) Milias-Argeitis, A., Summers, S., Stewart-Ornstein, J., Zuleta, I., Pincus, D., Lygeros, J., El Samad, H., and Khammash, M. (2011) *In silico* feedback for *in vivo* regulation of a gene expression circuit. *Nat. Biotechnol. 29*, 1114−1116.

(10) Whitaker, W. R., Davis, S. A., Arkin, A. P., and Dueber, J. E. (2012) Engineering robust control of two-component system phosphotransfer using modular scaffolds. *Proc. Natl. Acad. Sci. U.S.A.*, 18090−18095.

(11) Skerker, J. M., Prasol, M. S., Perchuk, B. S., Biondi, E. G., and Laub, M. T. (2005) Two-Component Signal Transduction Pathways Regulating Growth and Cell Cycle Progression in a Bacterium: A System-Level Analysis. *PLoS Biol. 3*, No. e334.

(12) Acharya, A., Ruvinov, S. B., Gal, J., Moll, J. R., and Vinson, C. (2002) A Heterodimerizing Leucine Zipper Coiled Coil System for Examining the Specificity of aPosition Interactions: Amino Acids I, V, L, N, A, and K. *Biochemistry 41*, 14122−14131.

(13) Whitaker, W. R., and Dueber, J. E. (2011) in *Synthetic Biology, Part A* (Voigt, C., Ed.), Vol. 497, pp 447−468, Methods in Enzymology; Academic Press, San Diego, CA.

(14) Whitaker, W. R. (2012) Engineering Modular Post-Translational Control Strategies in Prokaryotes. PhD Thesis, UC Berkeley, USA, 1−151.

(15) Zhu, Y., and Inouye, M. (2002) The role of the G2 box, a conserved motif in the histidine kinase superfamily, in modulating the function of EnvZ. *Mol. Microbiol. 45*, 653−663.

(16) Andersen, J. B., and Molin, S. (1998) New Unstable Variants of Green Fluorescent Protein for Studies of Transient Gene Expression in Bacteria. *Appl. Environ. Microbiol. 64*, 2240−2246.

(17) Nagai, T., Ibata, K., Park, E. S., Kubota, M., Mikoshiba, K., and Miyawaki, A. (2002) A variant of yellow fluorescent protein with fast and efficient maturation for cell-biological applications. *Nat. Biotechnol. 20*, 87−90.

(18) Shaner, N. C., Campbell, R. E., Steinbach, P. A., Giepmans, B. N. G., Palmer, A. E., and Tsien, R. Y. (2004) Improved monomeric red, orange and yellow fluorescent proteins derived from Discosoma sp. red fluorescent protein. *Nat. Biotechnol. 22*, 1567−1572.

(19) de los Santos, E. L., Hsiao, V., and Murray, R. M. (2013) Design and implementation of a biomolecular circuit for tracking protein concentration. *Proc. Am. Control Conf.*, 1−5.

(20) Pazy, Y., Wollish, A. C., Thomas, S. A., Miller, P. J., Collins, E. J., Bourret, R. B., and Silversmith, R. E. (2009) Matching Biochemical Reaction Kinetics to the Timescales of Life: Structural Determinants That Influence the Autodephosphorylation Rate of Response Regulator Proteins. *J. Mol. Biol. 392*, 1205−1220.

(21) Groban, E. S., Clarke, E. J., Salis, H. M., Miller, S. M., and Voigt, C. A. (2009) Kinetic Buffering of Cross Talk between Bacterial Two-Component Sensors. *J. Mol. Biol. 390*, 380−393.

(22) Solomaha, E., Szeto, F. L., Yousef, M. A., and Palfrey, H. C. (2005) Kinetics of Src homology 3 domain association with the proline-rich domain of dynamins: specificity, occlusion, and the effects of phosphorylation. *J. Biol. Chem. 280*, 23147−23156.

(23) Huang, C.-Y. F., and Ferrell, J. E., Jr. (1996) Ultrasensitivity in the mitogen-activated protein kinase cascade. *Proc. Natl. Acad. Sci. U. S. A. 93*, 10078−10083.

(24) Posern, G., Zheng, J., Knudsen, B. S., Kardinal, C., Muller, K. B., Hanafusa, H., and Feller, S. M. (1998) Development of highly selective SH3 binding peptides for Crk and CRKL which disrupt Crk-complexes with DOCK180, SoS and C3G. *Oncogene 16*, 1903−1912.

(25) Grunberg, R., Ferrar, T. S., van der Sloot, A. M., Constante, M., and Serrano, L. (2010) Building blocks for protein interaction devices. *Nucleic Acids Res. 38*, 2645−2662.

(26) Good, M. C., Zalatan, J. G., and Lim, W. A. (2011) Scaffold Proteins: Hubs for Controlling the Flow of Cellular Information. *Science 332*, 680−686.

(27) Munsky, B., Trinh, B., and Khammash, M. (2009) Listening to the noise: Random fluctuations reveal gene network parameters. *Mol. Syst. Biol. 5*, No. 318.

(28) Farrell, C. M., Grossman, A. D., and Sauer, R. T. (2005) Cytoplasmic degradation of ssrA-tagged proteins. *Mol. Microbiol. 57*, 1750−1761.

(29) Park, S.-H., Zarrinpar, A., and Lim, W. A. (2003) Rewiring MAP Kinase Pathways Using Alternative Scaffold Assembly Mechanisms. *Science 299*, 1061−1064.

(30) Bashor, C. J., Helman, N. C., Yan, S., and Lim, W. A. (2008) Using Engineered Scaffold Interactions to Reshape MAP Kinase Pathway Signaling Dynamics. *Science 319*, 1539−1543.

(31) Dueber, J. E., Wu, G. C., Malmirchegini, G. R., Moon, T. S., Petzold, C. J., Ullal, A. V., Prather, K. L. J., and Keasling, J. D. (2009) Synthetic protein scaffolds provide modular control over metabolic flux. *Nat. Biotechnol. 27*, 753−759.

(32) Moon, T. S., Dueber, J. E., Shiue, E., and Prather, K. L. J. (2010) Use of modular, synthetic scaffolds for improved production of glucaric acid in engineered *E. coli*. *Metab Eng. 12*, 298−305.

(33) Bessho, Y. (2003) Oscillations, clocks and segmentation. *Curr. Opin. Genet. Dev. 13*, 379−384.

(34) Imayoshi, I., Isomura, A., Harima, Y., Kawaguchi, K., Kori, H., Miyachi, H., Fujiwara, T., Ishidate, F., and Kageyama, R. (2013) Oscillatory control of factors determining multipotency and fate in mouse neural progenitors. *Science 342*, 1203−1208.

(35) Cai, L., Dalal, C. K., and Elowitz, M. B. (2008) Frequency-modulated nuclear localization bursts coordinate gene regulation. *Nature 455*, 485−490.